RSC Advances

PAPER

View Article Online
View Journal | View Issue

Cite this: *RSC Adv.*, 2024, **14**, 35232

An electrochemiluminescence device for visualized detection of lead in practical samples†

Huaanzi Hu, ‡[a] Cheng Wang, ‡[b] Chen Qian,*[c] Chengqi Li,[d] Yulin Li,[d] Jianbin Pan*[e] and Xinye Ni*[a]

Received 8th August 2024
Accepted 15th October 2024

DOI: 10.1039/d4ra05742b

rsc.li/rsc-advances

Lead (Pb^{2+}) pollution poses a significant threat to human health due to its potential accumulation through the food chain. In response to this challenge, an array of electrochemiluminescence (ECL) devices has been developed for the accurate and visualized detection of trace Pb^{2+}, achieving an ultra-low limit of detection (LOD) of 9.8 pg L^{-1}. The device utilizes a Pb^{2+}-specific aptamer DNA chain, modified on gold nanoparticles (AuNPs), to create an efficient ECL probe. The integration of this ECL probe into an indium tin oxide (ITO) substrate results in a Pb^{2+} specific array device. With the assistance of an up-response ECL imaging system, this setup enables the accurate and visualized determination of trace Pb^{2+}, not only in standard solution containing interference ions, but also in practical samples of *Lycium ruthenicum* Murr., *Glycyrrhiza uralensis* and lake water. This work advances the visual detection of Pb^{2+} using ECL-based technology, demonstrating significant potential for enhancing food safety.

1 Introduction

Lead (Pb) contamination poses a significant threat to both the environment and human health.[1,2] The contamination is primarily attributed to anthropogenic activities, such as mining, smelting, and the use of lead in various industrial products, including batteries and paints.[3] This toxic metal, although naturally occurring in trace amounts in the Earth's crust, has experienced a substantial increase in global production due to the high demand for automobile and mobile phone batteries.[4] The presence of Pb ions (Pb^{2+}) in soil, water, and air has increased significantly, leading to widespread food contamination.[5–7] The hazards of Pb^{2+} pollution are multifaceted, affecting both ecosystems and human health. In the environment, Pb^{2+} disrupts the natural balance by contaminating soil and water sources and biomagnifying through food chains, which poses a significant risk to flora and fauna.[8,9] For humans, Pb^{2+} contamination in foods can result in severe toxicity, posing significant health risks to the population. Children and developing fetuses are particularly vulnerable, as Pb^{2+} exposure can lead to impaired cognitive development and intellectual decline.[10] It also has detrimental effects on the cardiovascular, renal, and immune systems.[11] Long-term exposure can lead to more severe health problems, including neurological disorders and cancer.[12] Therefore, there is an urgent need to develop a device that can afford convenient and sensitive detection of Pb^{2+}.[13,14]

As a quintessential heavy metal, lead (Pb^{2+}) detection often relies on traditional methods such as Atomic Absorption Spectroscopy (AAS) and its advanced form, Electrothermal Atomic Absorption Spectroscopy (ET-AAS), which is known for their sensitivity and accuracy but require skilled technicians and can be time-consuming. Inductively Coupled Plasma Mass Spectrometry (ICP-MS) offers high sensitivity and a wide dynamic range, yet it is associated with higher costs and necessitates complex sample preparation.[15,16] In contrast, emerging nanomaterial-based sensors provide a promising alternative. These sensors leverage the high surface reactivity, large surface area, strong adsorption capacity, and high catalytic efficiency of nanomaterials to significantly enhance sensitivity and selectivity.[17] In recent years, the introduction of nanotechnology for the detection of Pb^{2+} is gaining increasing attentions.[18,19] Among these approaches, electrochemiluminescence (ECL) detection stands out due to its low background interference, rapid response, high precision, and portability, which led to the widespread adoption of the ECL method for the precise quantification of lead ions.[20–23] However, most of the current studies

[a]*Department of Radiotherapy, the Affiliated Changzhou No. 2 People's Hospital of Nanjing Medical University, Changzhou Medical Center, Nanjing Medical University, Changzhou 213003, P. R. China. E-mail: nxy@njmu.edu.cn*

[b]*School of Pharmacy, Changzhou University, No. 21 Middle Gehu Road, Changzhou, 213164, P. R. China*

[c]*Department of Orthopedics, Wujin Hospital Affiliated with Jiangsu University, Changzhou 213164, P. R. China. E-mail: qianchen88@126.com*

[d]*State Key Laboratory of Radiation Medicine and Protection, School for Radiological and Interdisciplinary Sciences (RAD-X), Soochow University, Suzhou 215123, P. R. China*

[e]*State Key Laboratory of Analytical Chemistry for Life Science, School of Chemistry and Chemical Engineering, Nanjing University, Nanjing 210023, P. R. China. E-mail: jbpan@nju.edu.cn*

† Electronic supplementary information (ESI) available. See DOI: https://doi.org/10.1039/d4ra05742b

‡ These authors contributed equally to this work.

fall short in providing a visualized method for the rapid and convenient assessment of Pb^{2+} levels in samples.

In response to this challenge, we have crafted a novel electrochemiluminescence (ECL) array system designed for the swift and clear identification of trace levels of Pb^{2+}. This system features a remarkably low detection limit and superior selectivity, making it an advanced tool for identifying Pb^{2+} with high precision and reliability. It is particularly suitable for monitoring Pb^{2+} in practical samples. Specifically, we have functionalized gold nanoparticles (AuNPs) with a specific sequence of aptamer DNA, creating an efficient Pb^{2+}-sensitive ECL probe designated as AuNPs@dsDNA. The $-NH_2$ groups within this construct serve as a co-reactant in the ECL reaction. The AuNPs, acting as the core material of the probe, facilitate electron transfer during the ECL process due to their excellent electrical conductivity. Additionally, the Au–S bonds guarantee that the DNA sequences attached to the AuNPs' surface remain stable in aqueous environments. This design ensures that the ECL signal from the probe-modified electrodes is robust and reliable. The probe can be integrated into an array of indium tin oxide (ITO) electrode tunnels, thereby forming a high-performance ECL detection platform. Concurrently, tris(2,2′-bipyridyl)ruthenium(II) dichloride ($Ru(bpy)_3Cl_2$), when dissolved in a phosphate-buffered saline (PBS) solution, acts as an ECL luminophore. In practical applications, Pb^{2+} from the sample selectively displaces the NH_2–ssDNA chains, thereby diminishing diminish the ECL signal from $Ru(bpy)_3Cl_2$. This interaction results in an exceptionally low limit of detection (LOD) for Pb^{2+} of 9.8 pg L^{-1}. To the best of our knowledge, this LOD represents one of the most sensitive detection limits reported for Pb^{2+} detection methodologies, as detailed in Table S1.† Moreover, the device is equipped with an ECL imaging system that enables the rapid and visual monitoring of Pb^{2+} at trace levels. In conclusion, the development of this ECL detector marks a significant advancement in the field of trace Pb^{2+} detection. It offers an efficient and precise method for the rapid assessment of Pb^{2+} concentrations, which is crucial for advancing related scientific research and holds substantial importance for ensuring food safety.

2 Experimental section

2.1 Preparation of array device for Pb^{2+} detection

A solution of AuNPs (10 μL) at a concentration of 25 nM was mixed with a tris(carboxyethyl)phosphine (TCEP) solution (20 μL) at 10 mM, along with a PBS solution (70 μL) at 0.01 M, within a 10 mL centrifuge tube. This mixture was thoroughly homogenized. Subsequently, 100 μL of a 12.5 μM chain A solution was introduced into the tube. Upon the addition of 1800 μL of *n*-butanol, the aqueous phase was carefully separated following a gentle centrifugation and adjusted to a final volume of 200 μL, yielding a concentration of 6.25 μM for the AuNPs@ssDNA solution. This resultant mixture was then applied to the array of ITO electrodes, with an aliquot of 10 μL dispensed into each tunnel. Once the electrodes were air-dried, chain B solution at a concentration of 25 μM was applied to the ITO electrodes, again using 10 μL per tunnel. After the ITO electrodes were fully dried, the assembly was completed, yielding an array of Pb^{2+} detection devices featuring the modified AuNPs@dsDNA.[24]

Chain A: 5′-GGTTGGTGTGGTTGGTTGGTGTGGTTGGTTGGTGTGGTTGGTTGGTGTGGTTGG-3′ modifications: 5′: SH C6.

Chain B: 5′-CAACC-3′ modifications: 5′: NH_2C6, 3′: NH_2C6.

2.2 Pb^{2+} detection and selectivity

A series of Pb^{2+} solutions with varying concentrations were applied to the array-based Pb^{2+} detection devices. After a 30 minute incubation period, the devices were rinsed with deionized water to remove any unbound species. For the preparation of the ECL reagent, 1 mL volume of a 10 mM $Ru(bpy)_3Cl_2$ solution was diluted to a final volume of 10 mL using a 0.1 M PBS solution (pH 7.4) within the measurement cell. The photomultiplier tube (PMT) was set to an operating voltage of 400 V, and the scanning rate for the potential was maintained at 100 mV s^{-1}. To assess the selectivity of the detection system, a range of potential interfering ions were tested,[25] including potassium (K^+), calcium (Ca^{2+}), sodium (Na^+), magnesium (Mg^{2+}), strontium (Sr^{2+}), mercury (Hg^{2+}), iron (Fe^{3+}), cadmium (Cd^{2+}), cesium (Cs^+), silver (Ag^+), and copper (Cu^{2+}). Each of these ions was present at a concentration of 100 μg L^{-1}, while the Pb^{2+} concentration was set at 100 ng L^{-1}. The procedure for these selectivity tests was conducted in accordance with the established protocol for Pb^{2+} detection.

3 Results and discussion

3.1 Characterization on structure and ECL activity

The AuNPs, with an average size of 5 nm, were commercially available and further functionalized to specifically detect Pb^{2+} by conjugating them with a DNA aptamer sequence (referred to as chain A), following established protocols.[26,27] The addition of TCEP facilitated the attachment of chain A to the AuNPs' surface. Successful functionalization was evidenced by a significant decrease in the zeta potential of the AuNPs@ssDNA compared to that of the pristine AuNPs, as depicted in Fig. 1A. Furthermore, the zeta potential of the AuNPs@dsDNA was notably lower than that of the AuNPs@ssDNA, confirming the formation of the duplex structure.

Cyclic voltammetry (CV) was employed to substantiate these modifications. The CV responses of glassy carbon electrodes (GCEs) modified with AuNPs, AuNPs@ssDNA, and AuNPs@dsDNA were recorded in a PBS solution containing 1 mM $Ru(bpy)_3Cl_2$ (Fig. 1B). The oxidation peak for $Ru(bpy)_3Cl_2$ was observed at approximately +1.30 V and was significantly enhanced upon AuNPs modification, indicating improved electrode conductivity due to the AuNPs. This peak was further intensified after the addition of chain A, resulting in AuNPs@ssDNA. The negative zeta potential of ssDNA (Fig. 1A) likely promoted electrostatic interactions with $Ru(bpy)_3Cl_2$, leading to the observed increase of current (Fig. 1B). Supporting evidence was provided by the CV data for ethylenediamine (Fig. S1†), which showed an oxidation peak at +1.35 V, akin to that of $Ru(bpy)_3Cl_2$. The comparison between AuNPs@dsDNA

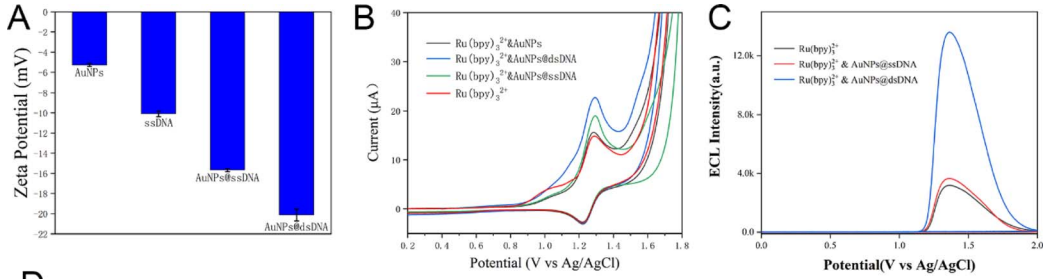

D

$$AuNPs@dsDNA\text{-}CH_2NH_2 - e^- \rightarrow AuNPs@dsDNA\text{-}CH_2NH_2^{\bullet+} \quad (1)$$

$$AuNPs@dsDNA\text{-}CH_2NH_2^{\bullet+} - H^+ \rightarrow AuNPs@dsDNA\text{-}^{\bullet}CH{=}NH_2^+ \quad (2)$$

$$Ru(bpy)_3^{2+} - e^- \rightarrow Ru(bpy)_3^{3+} \quad (3)$$

$$Ru(bpy)_3^{3+} + AuNPs@dsDNA\text{-}^{\bullet}CH{=}NH_2^+ \rightarrow Ru(bpy)_3^{2+*} + AuNPs@dsDNA\text{-}CH{=}NH_2^+ \quad (4)$$

$$Ru(bpy)_3^{2+*} \rightarrow Ru(bpy)_3^{2+} + h\nu \quad (5)$$

Fig. 1 (A) The zeta potential for AuNPs, chain A, AuNPs@ssDNA (AuNPs modified with chain A) and AuNPs@dsDNA (AuNPs@ssDNA further modified with chain B); (B) the CV data of GCE modified with $Ru(bpy)_3Cl_2$ solution (blank), AuNPs, AuNPs@ssDNA and AuNPs@dsDNA. (C) The ECL data for ITO electrodes modified with $Ru(bpy)_3Cl_2$ solution (blank), AuNPs, AuNPs@ssDNA and AuNPs@dsDNA. The CV and ECL measurements were conducted in 0.1 M PBS (pH = 7.4) solution with 1 mM $Ru(bpy)_3^{2+}$. The PMT was set at 400 V with scan rate of 100 mV s^{-1}. (D) The proposed ECL mechanism for the device.

and AuNPs@ssDNA in Fig. S2 and S3† further corroborated the role of $-NH_2$ groups in enhancing the oxidation peak of AuNPs@dsDNA, and the increased DNA content and $Ru(bpy)_3Cl_2$ intercalation into dsDNA, respectively.

The ECL emission peak of $Ru(bpy)_3Cl_2$ was detected at around +1.40 V, with an onset potential of +1.08 V (Fig. 1C). This signal was notably enhanced upon the modification with AuNPs@ssDNA (Fig. 1C), potentially due to the increased current observed in Fig. 1B. A marked enhancement in the ECL signal was observed upon the addition of NH_2–ssDNA (chain B) to AuNPs@ssDNA, highlighting the reactivity of $-NH_2$ groups (Fig. 1C). The ECL peak at +1.40 V mirrored the oxidation peak of $Ru(bpy)_3Cl_2$, suggesting that the ECL signal is a result of the oxidation of $Ru(bpy)_3Cl_2$. The proposed ECL mechanism is illustrated in Fig. 1D.

3.2 Detection mechanism of Pb^{2+}

ITO electrodes offer distinct benefits over conventional GCEs, including ease of fabrication, integration potential, and superior light transmission capabilities for ECL imaging assessments. These attributes make ITO electrodes a promising platform for the development of visual detection devices for Pb^{2+}. To facilitate rapid and visual Pb^{2+} monitoring, an array of Pb^{2+} detection devices was fabricated by immobilizing AuNPs@dsDNA within the arrayed tunnel structures of the ITO electrode (as depicted in Fig. 2A). The ECL responses from these devices, upon exposure to Pb^{2+} solutions of varying concentrations, were recorded in a 0.1 M PBS solution containing 1 mM $Ru(bpy)_3Cl_2$ (Fig. 2B). A progressive decrease in ECL signals was observed as Pb^{2+} concentrations rose from 0 to 10 μg L^{-1}. The ECL intensity exhibited a strong linear relationship with the logarithmic concentration of Pb^{2+}, yielding a low limit of detection (LOD) for Pb^{2+} at 9.8 pg L^{-1} (Fig. 2C). The observed reduction in ECL signal is attributed to the displacement of NH_2–ssDNA by Pb^{2+}. To elucidate this mechanism, the CV of the Pb^{2+} detection devices was measured before and after exposure to Pb^{2+} solutions in a 0.1 M PBS solution containing 1 mM $Ru(bpy)_3Cl_2$ (Fig. 2D). A noticeable decrease in the oxidation peak current of the AuNPs@dsDNA-modified GCEs was observed post-Pb^{2+} treatment, aligning with the current levels of AuNPs@ssDNA (as indicated by the blue line in Fig. 2D). This finding provides corroborative evidence for the proposed displacement mechanism.

To assess the selectivity of the probe, a panel of common interfering ions were tested at concentrations 1000-fold higher than that of Pb^{2+} (Fig. 2E). The selection encompassed both ubiquitous environmental cations and representative heavy metal ions, given Pb^{2+} is classified as a heavy metal. The Pb^{2+} detection devices demonstrated exceptional selectivity for Pb^{2+}, underscoring their reliability and potential for practical Pb^{2+} detection applications.

Moreover, to prove its storage stability, we have conducted a comparative experiment on two batches of device, one is freshly prepared device while another is old device stored for one month under room temperature. As shown in Fig. S4,† we can see that both batches of device maintain similar ECL response to the same sample, suggesting the high storage stability of the device.

3.3 Visualized detection of Pb^{2+}

Additionally, the incorporation of ECL imaging technology has been employed to facilitate the rapid and visual monitoring of

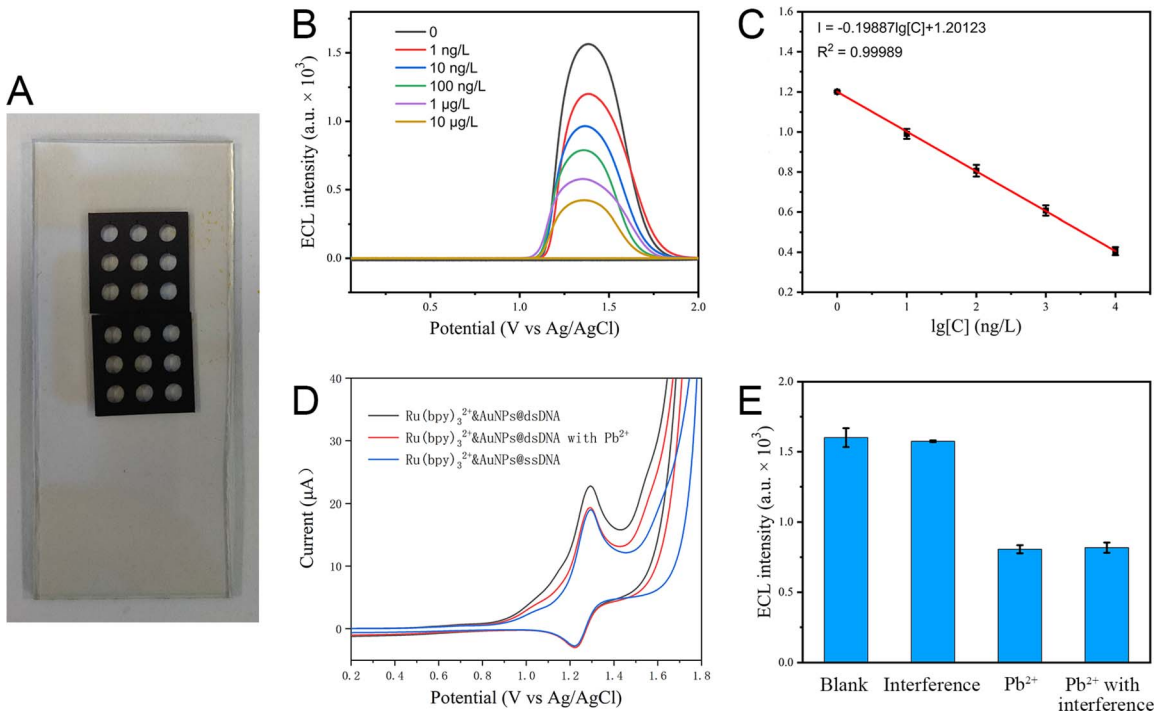

Fig. 2 (A) A visual representation of the ITO electrodes modified with AuNPs@dsDNA, which serve as part of an array device designed for the visual detection of Pb^{2+}; (B) the ECL signals of array devices treated by various standard Pb^{2+} concentrations. (C) The calibration curve between the ECL intensity and the concentration (expressed as logarithm value) of Pb^{2+}; (D) the CV of GCE modified with AuNPs@ssDNA and AuNPs@dsDNA treated with or without 100 ng L^{-1} of Pb^{2+}; (E) assessment of resistance to interference of the Pb^{2+} detection array device. The CV and ECL measurements were conducted in 0.1 M PBS (pH = 7.4) solution with 1 mM $Ru(bpy)_3^{2+}$. The PMT was set at 400 V with scan rate of 100 mV s^{-1}. For the interference assay, the Pb^{2+} concentration was 100 ng L^{-1} while the interference ions were fixed at an equal concentration of 100 μg L^{-1}.

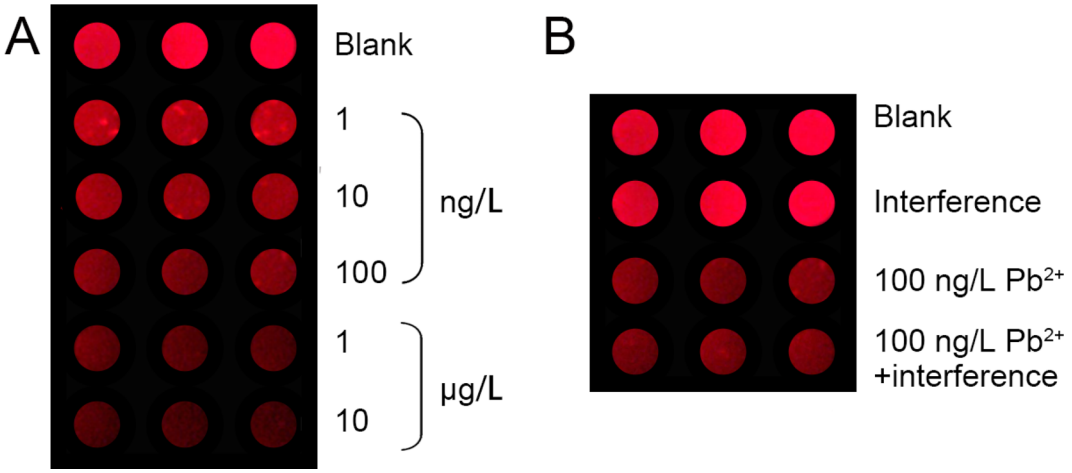

Fig. 3 The visualization of Pb^{2+} by the device. (A) The device response upon treatment with Pb^{2+} solutions across varying concentrations, illustrating dose-dependent ECL intensity changes; (B) the selectivity assessment in the presence of different designated interfering ions, confirming minimal cross-reactivity. All scans were conducted at a rate of 400 mV s^{-1}.

Pb^{2+} in practical samples, as depicted in Fig. 3. The array of Pb^{2+} detection devices exhibit vivid red ECL emissions, which are indicative of the luminescence generated by $Ru(bpy)_3Cl_2$. A discernible reduction in ECL intensity is observed as the Pb^{2+} concentration escalates from 1 ng L^{-1} to 10 μg L^{-1}, paralleling the trend previously illustrated in Fig. 2B and C. Concurrently, the findings in Fig. 3B corroborate the high selectivity of this ECL-based device for Pb^{2+} detection. These outcomes underscore the device's efficacy and potential in providing precise and visual Pb^{2+} monitoring in food samples.

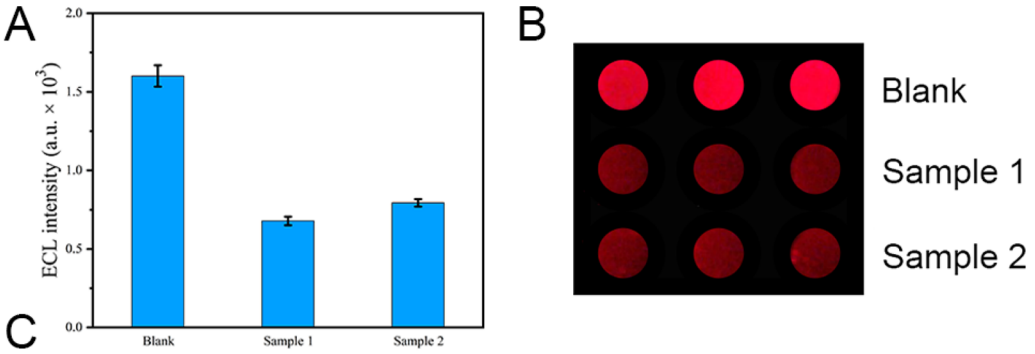

	ECL	ICP-MS
Lycium ruthenicum Murr. from Qinghai (Sample 1)	168.9 ng/g (R.S.D.:2.8%)	225.9 ng/g (R.S.D.:0.5%)
Lycium ruthenicum Murr. from Xinjiang (Sample 2)	44.9 ng/g (R.S.D.:2.3%)	43.1 ng/g (R.S.D.:2.9%)

Fig. 4 The detection performance of the device on practical food samples. (A) The ECL signal of the device in response to the different practical samples; (B) ECL images of the device in response different practical samples; (C) the summary of Pb^{2+} concentration in different practical samples determined by our device and ICP-MS.

3.4 The detection performance of the device on practical samples

Lycium ruthenicum Murr., recognized for its rich content of anthocyanins, which provides exceptional antioxidant capabilities, is crucial for developing functional foods and beverages that promote health. Its use in traditional medicine and ongoing research into its phytochemicals further enhance its role in creating innovative, health-beneficial food products.[28] Consequently, the development of a swift, quantitative, and visual analytical method for detecting Pb^{2+} contamination in *Lycium ruthenicum* Murr. is of paramount importance to ensure its safety for food and medicinal application. To verify the practicability of the Pb^{2+} detection device, we applied it to the quantitative analysis of Pb^{2+} in *Lycium ruthenicum* Murr. from

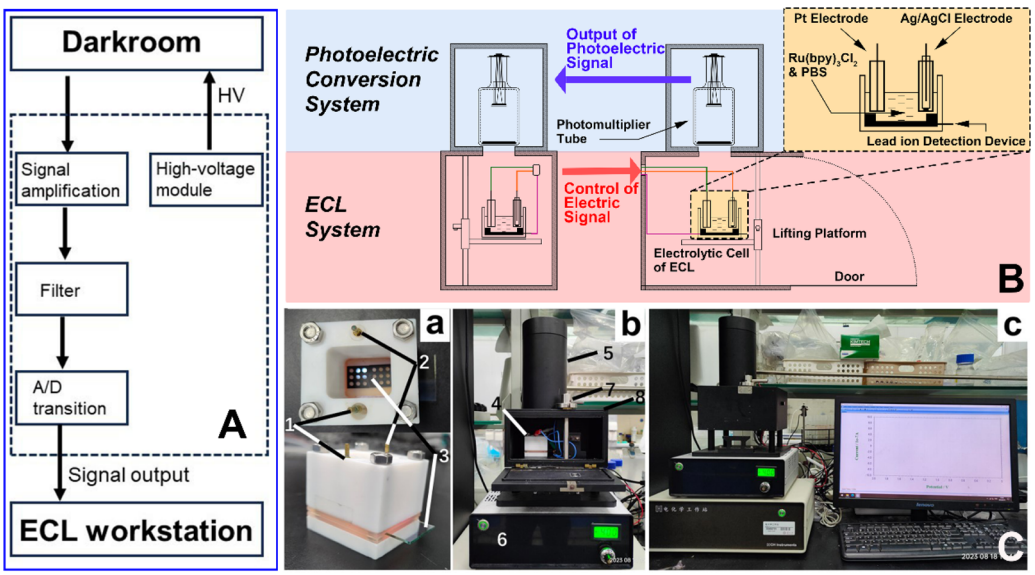

Fig. 5 (A) The schematic structure of the controller in ECL detection system. (B) The schematic structure of the newly designed ECL detector. (C) The practical picture and corresponding illustration of the ECL detector (a) the measuring pool for ITO electrode based Pb^{2+} detection devices: (1) counter electrode (Pt), (2) reference electrode (Ag/AgCl), (3) working electrode (ITO electrode based Pb^{2+} detection device); (b) newly designed ECL detector: (4) measuring pool, (5) PMT, (6) controller, (7) lock, (8) darkroom; (c) the practical application of this instrument in ECL detection using ITO electrodes.

Qinghai (sample 1) and Xinjiang (sample 2) respectively. It was found that the ECL signal was significantly quenched in both groups of samples (Fig. 4A and B). Quantitative analysis of Pb^{2+} content in *Lycium ruthenicum* Murr. showed that the contents of sample 1 and sample 2 were 168.9 ng g^{-1} and 44.9 ng g^{-1}, respectively. In comparison with the ICP-MS method (Fig. 4C), the concentration of Pb^{2+} in sample 1 and sample 2 were 225.9 ng g^{-1} and 43.1 ng g^{-1}, respectively, which is consistent with the results measured by our DNA-based biosensor. To further confirm the detection capability of our device, we also introduced two more practical samples, *Glycyrrhiza uralensis* from Inner Mongolia and lake water from Dushu lake, as representative food and environmental samples. As shown in Fig. S5,† our device can give comparable results to ICP-MS at higher Pb^{2+} condition while remain sensitive under lower Pb^{2+} condition where ICP-MS is unapplicable. These results demonstrate that our device can accurately detect trace amounts of Pb^{2+} in real samples. Therefore, it is of special significance that this device can effectively identify potential trace Pb^{2+} contamination in practical objects at an early stage, thereby enhancing human health.

In alignment with the practical application requirements for Pb^{2+} detection, we have engineered a corresponding ECL detection apparatus, which encompasses a control module (as shown in Fig. 5A) and an up-response ECL detection component (illustrated in Fig. 5B). The physical images of the system are displayed in Fig. 5C, with photographs (a) and (b) showcasing the device's distinct parts. Integrated with an electrochemical workstation, this ECL detection setup is capable of delivering consistent CV and ECL signals when used with ITO electrodes, as depicted in picture (c) of Fig. 5C. This newly crafted system has been effectively utilized for Pb^{2+} detection in the current study. The array-based Pb^{2+} detection device, which emits ECL signals in an upward direction, is particularly compatible with the up-response ECL detector, offering a distinct advantage over GCE setups.

4 Conclusions

In conclusion, this study presents a groundbreaking array ECL device for the ultra-sensitive and selective detection of Pb^{2+} in practical samples, addressing a critical need in food safety. By leveraging the unique properties of AuNPs modified with a Pb^{2+}-specific aptamer DNA chain, the device achieves an unprecedented low LOD of 9.8 pg L^{-1}, significantly outperforming existing technologies. The innovative integration of this ECL probe into an ITO electrode array allows for rapid and visualized detection, with high selectivity and short measurement times, making it suitable for on-site monitoring of trace Pb^{2+}. The successful application of the device in multiple practical samples, demonstrates its practicality and potential for early identification of Pb^{2+} contamination, thereby enhancing food safety. Moreover, the newly designed ECL detection system, with its controller and up-response ECL detector, ensures stable and efficient operation, showcasing the device's readiness for field applications. This work not only advances the field of trace heavy metal ECL detection but also provides a vital tool for monitoring trace Pb^{2+} concentrations, playing a key role in promoting relevant research and safeguarding public health.

However, the preparation of the ECL detection system involves multiple steps, including the functionalization of AuNPs with aptamer DNA and the assembly of the ITO electrode array. This complexity may pose challenges in scaling up. Therefore, in our future work, we will focus on simplifying the preparation procedure to improve its reproducibility and reliability for potential widespread use or commercial applications. Moreover, the ECL detection system requires a custom-designed apparatus, including an electrochemical workstation and a specialized ECL detector. Therefore, our future work focus also includes miniaturizing and marketization of this detection equipment to improve its accessibility for laboratories or field applications.

Data availability

The data supporting this article have been included as part of the ESI.†

Conflicts of interest

There are no conflicts to declare.

Acknowledgements

Our project was supported by the grant from the Jiangsu Provincial Outstanding Postdoctoral Program (Grant No. 2022ZB823), the National Key Research and Development Program of China (no. 2022YFD17800). We acknowledge the ICP-MS analysis provided by from Shiyanjia Lab (**https://www.Shiyanjia.com**) and SCI-GO (**https://www.ceshigo.com/**). During the preparation of this work the authors used Kimi AI (**https://kimi.moonshot.cn/**) to improve readability and language. After using this tool/service, the authors reviewed and edited the content as needed and take full responsibility for the content of the publication.

Notes and references

1 M. Komárek, V. Ettler, V. Chrastný and M. Mihaljevič, Lead isotopes in environmental sciences: a review, *Environ. Int.*, 2008, **34**(4), 562–577.
2 S. Tong, Y. E. v. Schirnding and T. Prapamontol, Environmental lead exposure: a public health problem of global dimensions, *Bull. World Health Organ.*, 2000, **78**(9), 1068–1077.
3 E. Obeng-Gyasi, Sources of lead exposure in various countries, *Rev. Environ. Health*, 2019, **34**(1), 25–34.
4 H. Cheng and Y. Hu, Lead (Pb) isotopic fingerprinting and its applications in lead pollution studies in China: a review, *Environ. Pollut.*, 2010, **158**(5), 1134–1146.
5 M. C. d. V. Neto, T. B. C. Silva, V. E. de Araujo and S. V. C. de Souza, Lead contamination in food consumed and produced in Brazil: systematic review and meta-analysis, *Food Res. Int.*, 2019, **126**, 108671.

6 H.-B. Li, M.-Y. Li, D. Zhao, Y.-G. Zhu, J. Li, A. L. Juhasz, X.-Y. Cui, J. Luo and L. Q. Ma, Food influence on lead relative bioavailability in contaminated soils: mechanisms and health implications, *J. Hazard. Mater.*, 2018, **358**, 427–433.

7 T. Morales-Silva, B. C. Silva, V. H. D. Silva and L. D. B. Faria, Simplification effect of lead soil contamination on the structure and function of a food web of plant-associated insects, *Agric. Ecosyst. Environ.*, 2023, **354**, 108570.

8 A. Kumar, A. Kumar, C.-P. Mms, A. K. Chaturvedi, A. A. Shabnam, G. Subrahmanyam, R. Mondal, D. K. Gupta, S. K. Malyan and S. S. Kumar, Lead toxicity: health hazards, influence on food chain, and sustainable remediation approaches, *Int. J. Environ. Res. Publ. Health*, 2020, **17**(7), 2179.

9 M. J. M. Notten, N. Walraven, C. J. Beets, P. Vroon, J. Rozema and R. Aerts, Investigating the origin of Pb pollution in a terrestrial soil–plant–snail food chain by means of Pb isotope ratios, *Appl. Geochem.*, 2008, **23**(6), 1581–1593.

10 X. Zeng, X. Huo, X. Xu, D. Liu and W. Wu, E-waste lead exposure and children's health in China, *Sci. Total Environ.*, 2020, **734**, 139286.

11 M. Boskabady, N. Marefati, T. Farkhondeh, F. Shakeri, A. Farshbaf and M. H. Boskabady, The effect of environmental lead exposure on human health and the contribution of inflammatory mechanisms, a review, *Environ. Int.*, 2018, **120**, 404–420.

12 K. Raj and A. P. Das, Lead pollution: impact on environment and human health and approach for a sustainable solution, *Environ. Chem. Ecotoxicol.*, 2023, **5**, 79–85.

13 M. S. Salman, H. Znad, M. N. Hasan and M. M. Hasan, Optimization of innovative composite sensor for Pb (II) detection and capturing from water samples, *Microchem. J.*, 2021, **160**, 105765.

14 Y. Zhang, C. Wu, H. Liu, M. R. Khan, Z. Zhao, G. He, A. Luo, J. Zhang, R. Deng and Q. He, Label-free DNAzyme assays for dually amplified and one-pot detection of lead pollution, *J. Hazard. Mater.*, 2021, **406**, 124790.

15 M. Arjomandi and H. Shirkhanloo, A review: analytical methods for heavy metals determination in environment and human samples, *Anal. Methods Environ. Chem. J.*, 2019, **2**(03), 97–126.

16 A. S. Maghsoudi, S. Hassani, K. Mirnia and M. Abdollahi, Recent advances in nanotechnology-based biosensors development for detection of arsenic, lead, mercury, and cadmium, *Int. J. Nanomed.*, 2021, **16**, 803–832.

17 L. Wang, X. Peng, H. Fu, C. Huang, Y. Li and Z. Liu, Recent advances in the development of electrochemical aptasensors for detection of heavy metals in food, *Biosens. Bioelectron.*, 2020, **147**, 111777.

18 F. Aboufazeli, H. R. L. Z. Zhad, O. Sadeghi, M. Karimi and E. Najafi, Novel ion imprinted polymer magnetic mesoporous silica nano-particles for selective separation and determination of lead ions in food samples, *Food Chem.*, 2013, **141**(4), 3459–3465.

19 H. Singh, A. Bamrah, S. K. Bhardwaj, A. Deep, M. Khatri, K.-H. Kim and N. Bhardwaj, Nanomaterial-based fluorescent sensors for the detection of lead ions, *J. Hazard. Mater.*, 2021, **407**, 124379.

20 Y. Wang, H. Shi, L. Zhang, S. Ge, M. Xu, X. Wang and J. Yu, Two-dimensional black phosphorus nanoflakes: a coreactant-free electrochemiluminescence luminophors for selective Pb^{2+} detection based on resonance energy transfer, *J. Hazard. Mater.*, 2021, **403**, 123601.

21 Y. He, X. X. Hu, Z. J. Gong, S. H. Chen and R. Yuan, A novel electrochemiluminescence biosensor based on the self-ECL emission of conjugated polymer dots for lead ion detection, *Microchim. Acta*, 2020, **187**, 8.

22 M. Li, Q. K. Kong, Z. Q. Bian, C. Ma, S. G. Ge, Y. Zhang, J. H. Yu and M. Yan, Ultrasensitive detection of lead ion sensor based on gold nanodendrites modified electrode and electrochemiluminescent quenching of quantum dots by electrocatalytic silver/zinc oxide coupled structures, *Biosens. Bioelectron.*, 2015, **65**, 176–182.

23 P. A. Jiang, L. J. Luo, X. H. Liu, W. L. Zhao, X. Y. Bi, L. Luo, L. B. Li and T. Y. You, A potential-resolved ratiometric electrochemiluminescence aptasensor for Pb2+: gold nanoclusters and amino-terminated perylene derivative as both emitters and resonance energy transfer donor-acceptor pair, *Sens. Actuators, B*, 2023, **386**, 8.

24 Z. Wang, Y. Li, J.-B. Pan, M. Xu, J.-J. Xu and D. Hua, Array electrochemiluminescence device with ultra-high sensitivity and selectivity for rapid visualized monitoring of trace radon in environment, *J. Hazard. Mater.*, 2023, **453**, 131449.

25 K. K. Harish, A. R. Nesaragi, N. K. Kalagatur, P. Naik, M. Madegowda, A. Pandith, K. A. Dahlous, S. Mohammad, H. P. Shivarudrappa, T. M. Sharanakumar and H. Guddappa, Imidazole-centred cupric ions sensor: experimental validation, theoretical understanding, and zebrafish bioimaging, *J. Photochem. Photobiol., A*, 2024, **452**, 115565.

26 W. Deng, L.-R. Hong, M. Zhao, Y. Zhuo and M. Gao, Electrochemiluminescence-based detection method of lead (II) ion via dual enhancement of intermolecular and intramolecular co-reaction, *Analyst*, 2015, **140**(12), 4206–4211.

27 Y. Hao, Y. Li, L. Song and Z. Deng, Flash synthesis of spherical nucleic acids with record DNA density, *J. Am. Chem. Soc.*, 2021, **143**(8), 3065–3069.

28 J. Zheng, C. Ding, L. Wang, G. Li, J. Shi, H. Li, H. Wang and Y. Suo, Anthocyanins composition and antioxidant activity of wild Lycium ruthenicum Murr. from Qinghai-Tibet Plateau, *Food Chem.*, 2011, **126**(3), 859–865.

